Appl. Phys. A (2015) 118:1015–1021
DOI 10.1007/s00339-014-8861-x

Applied Physics A
Materials Science & Processing

Multi-particle FEM modeling on microscopic behavior of 2D particle compaction

Y. X. Zhang · X. Z. An · Y. L. Zhang

Received: 17 April 2014 / Accepted: 27 October 2014 / Published online: 8 November 2014

Abstract In this paper, the discrete random packing and various ordered packings such as tetragonal and hexagonal close packed structures generated by discrete element method and honeycomb, which is manually generated were input as the initial packing structures into the multi-particle finite element model (FEM) to study their densification during compaction, where each particle is discretized as a FEM mesh. The macro-property such as relative density and micro-properties such as local morphology, stress, coordination number and densification mechanism obtained from various initial packings are characterized and analyzed. The results show that the coupling of discrete feature in particle scale with the continuous FEM in macro-scale can effectively conquer the difficulties in traditional FEM modeling, which provides a reasonable way to reproduce the compaction process and identify the densification mechanism more accurately and realistically.

1 Introduction

In the past decades, powder metallurgy (PM) has been increasingly used in manufacturing a variety of products, especially in the production of automotive parts such as gears and cams as a net shape process. The advantages of PM technique lie in its cost-effective, materials saving, easy operation, environment friendly, high production rate and net shape or near net shape forming for complex geometrical and structural metals or alloys with high melting point or porous structures, which make it very competitive with conventional metallurgical producing processes such as casting or other processes such as forging and machining [1, 2]. Nowadays, besides the manufacturing of complicated and specially required structural parts, PM has been gradually extended to the production of advanced functional materials [3–7]. Among PM production processes, powder cold compaction which is one of the major stages plays a key role, since highly dense and uniform compacts are the precondition for high-performance products. Therefore, a large variety of studies in the past were carried out in this regards both physically and numerically.

It is known that the evolution of local relative density and stress distribution in the green compacts, which are critical parameters in determining PM component quality and properties, is very difficult to characterize in situ in physical experiments. This barrier can be conquered by computer simulations, among which finite element method (FEM) is effective in dealing with this problem, and various models were proposed and incorporated into this method. In this aspect, the powders are considered to be the continuous body. Normally, two kinds of continuous models are used in FEM simulation. One is the micro-mechanical model [8–15]; in this model, the granular dynamics are given by uniform strain field, which assumes that the motion of each particle is governed by macroscopic strain field. Therefore, the particles keep indention with each other, no local rearrangement and rotation are considered, which is different from real process [16]. Another one to describe the properties of powdered material is the empirical model (phenomenological model) [17–25], in which some functions are used to describe the response of porous materials upon the stress and also the relative density distribution and impact load in the final product can be predicted [26, 27]. Even though above information is

Y. X. Zhang · X. Z. An (✉) · Y. L. Zhang
School of Materials and Metallurgy, Northeastern University, Shenyang 110004, People's Republic of China
e-mail: anxz@mail.neu.edu.cn

important in process design and optimization, however, it cannot accurately predict the impact mechanical properties, especially in cold powder compaction because the geometry and physics of the compacts are ignored. Although a large number of constitutive models for powder densification are available in macroscopic FEM simulation, there are few that can consider the discrete particle features (e.g., particle shape, size and distribution and particle microstructure), which are the key parameters in determining the compact quality, and the high-performance powder compacts are really hard to be realized in traditional FEM continuous modeling. The disadvantage of FEM modeling can be compensated by the so-called discrete element method (DEM) simulation, which has been successfully used in our previous work on the packing densification of coarse particles [28–30]. And now, it has also been applied in modeling the compaction of fine powders [31–36], however, its effectiveness is mostly limited to the small deformation of powders with the relative density lower than about 0.85 [37, 38].

Recently, a multi-particle finite element method (MPFEM) was proposed to consider the particle discrete characteristics and the continuous bulk properties of powders. In MPFEM simulation, individual particle discretized with a finite element mesh allows for a full description of the densification mechanism. With this method, PavanaChand and KrishnaKumar [39] modeled the compaction of two spheres. Lee et al. [40] studied the compaction of two-dimensional (2D) aluminum powders under different pressing conditions. However, no systematic studies were found on the compaction of powders by using MPFEM simulation, especially the micro-dynamic analysis on the compaction process, and corresponding densification mechanisms for different initial packings are still lacking.

In this paper, we carried out MPFEM simulation in 2D on the densification of equal spheres subjected to uniaxial die compaction. Different initial packings for copper powders, which include random loose packing and various ordered packing structures such as tetragonal packing, hexagonal close packed (HCP) structure and honeycomb packing before compaction were generated and input in the FEM model. Then, each discrete structure was densified under single action die compaction. Dynamic compaction processes were characterized, and the densification mechanisms of different compacts were identified and analyzed based on the pore filling and particle mass transfer from particle scale.

2 Simulation model and conditions

We coupled DEM and FEM method from particle scale to analyze the single action die compaction of equal disks of copper (with the diameter $d = 2$ mm) under quasi-static conditions using the explicit integration scheme of a commercial finite element program (MSC. Marc). The number of particles which can be handled efficiently is determined by the CPU speed and RAM restrictions in addition to the number of particle–particle contact pairs. The mesh division of each discretized particle in the initial packing is shown in Fig. 1, totally 300 finite elements and 321 nodes are included.

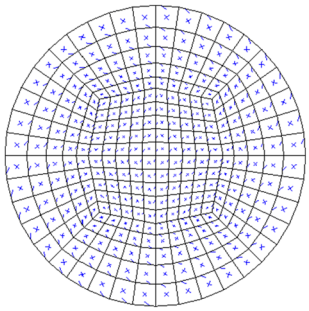

Fig. 1 Mesh division for each particle before compaction in FEM simulation

Four initial packings with random and different ordered packing structures (except honeycomb packing which is manually generated) were generated by DEM simulation. The relative packing density ρ and the number of particles N in each structure are listed as: (a) random packing, $\rho = 0.691$, $N = 65$; (b) tetragonal packing, $\rho = 0.782$, $N = 16$; (c) hexagonal close packing, $\rho = 0.876$, $N = 20$; and (d) honeycomb packing, $\rho = 0.602$, $N = 80$.

Typical DEM simulations are performed with periodic conditions or application of macroscopic strain/stress on a peripheral layer of particles. This method of applying periodic boundary condition cannot be efficiently duplicated in FEM. As an alternative, the boundary conditions of the simulations are summarized as follows. Displacement boundary conditions are imposed via rigid walls. In simulation, the position of die wall is fixed. And the change in density of the compact was determined by the change in displacement of the upper punch. The top side of the compact moves closer at an assumed strain rate. Referring to the statistic of coordination number (CN), contact with the wall is equal to contact with the particles. The simulation results are not affected by the strain rate since materials are assumed to be not strain rate sensitive. Inertia of the system is also checked during the simulations to avoid any dynamic effect caused by large strain rate.

The particles are constitutively assumed as elastic–plastic material. The elastic–plastic model has been frequently and successfully used for the numerical simulation of most metallic solids such as copper, iron/steel, aluminium and lead in FEM modeling for years [16, 40–43]. We

use copper particles with the properties of Young's modulus $E = 120$ GPa, Poisson's ratio $v = 0.3$, strength coefficient $K = 448$ MPa, work hardening index $m = 0.126$ and the friction coefficient among particles and between particles and the punch is set to be $\mu = 0.2$ with Coulomb friction model being used. The die wall is rigid and set to be smooth to reduce wall friction effect. No interparticle cohesion was considered due to restrictions in the FEM software used. Although cohesion may affect the post compaction properties, it is still argued that for the monotonic loading response to densification, cohesion effect is not so significant [44]. During simulation, the contact between particles, which has been regarded as an important issue in DEM and DDA modeling [28, 45], is checked automatically and dynamically by software embedded algorithm at each modeling step to guarantee the convergence of the results and precision.

It is worth to mention that our current work is mainly focusing on the compaction of spherical particles, which is relatively easy to construct different initial packing structures dynamically by DEM modeling in terms of particle position and diameter. On this basis, the MPFEM numerical simulation on the compaction of some convex platonic polyhedra such as tetrahedra, cubes and octahedra is undergoing. In our future work, the study will be extended to the packing densification of concave particles or particles with more complicated geometry, which tends to be more challenging with the difficulties in producing different ordered and disordered initial packings in DEM simulation and subsequent compaction due to the irregular particle shape and complex interaction mechanism between particles.

3 Results and discussion

3.1 Comparison between our numerical and physical results

Among many factors, which can create effects on the compaction, the compression pressure P plays a dominant role. Here, P is referred to as the average pressure, which is determined by the displacement of the punch. Figure 2 shows the relationship between pressure P and relative density ρ from both our numerical simulation and physical experiments. It can be seen that similar trends can be observed, i.e., for each P-ρ curve, P increases slowly when ρ is small; however, when ρ is high (e.g., $\rho > 0.85$), there is a rapid increase for P. At very high relative density (e.g., $\rho > 0.95$), the three P-ρ curves from numerical simulations tend to be coincided. In this case, the densification of the compact has transmitted from deformation of individual particles to bulk behavior, which shows the property of

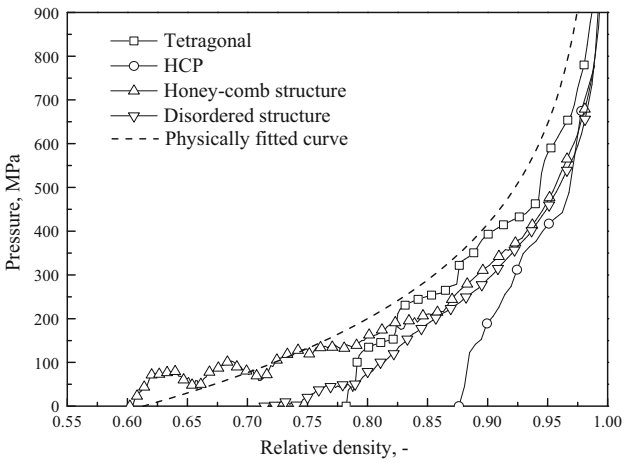

Fig. 2 Comparison of pressure-relative density relations between numerical simulation and physical experiments

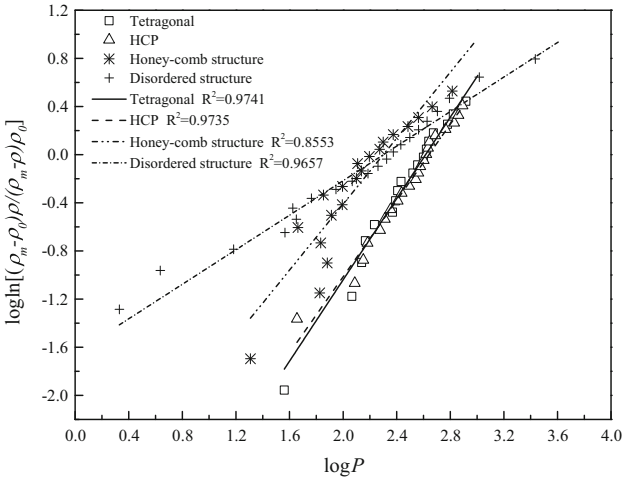

Fig. 3 Fitting of the simulation results obtained from four initial packing structures with double logarithmic equation

fully dense metal. Meanwhile, the slightly lower of our numerical curves than the physical experiments showing in Fig. 2 can be ascribed to: (a) The friction between the particles and the die wall is ignored and (b) the simulation results are obtained from 2D other than the 3D powder compaction in physical experiments. Anyhow, the qualitative agreement between our numerical results and physical results implies the validity of our proposed model.

In addition, our numerical results are also fitted by double logarithmic equation given by:

$$m\log\ln\frac{(\rho_m-\rho_0)\rho}{(\rho_m-\rho)\rho_0}=\log P-\log M,$$

where ρ_m—density of fully dense metal, ρ_0—initial packing density of the compact, ρ—relative density of the compact, P—compaction pressure, M—compaction

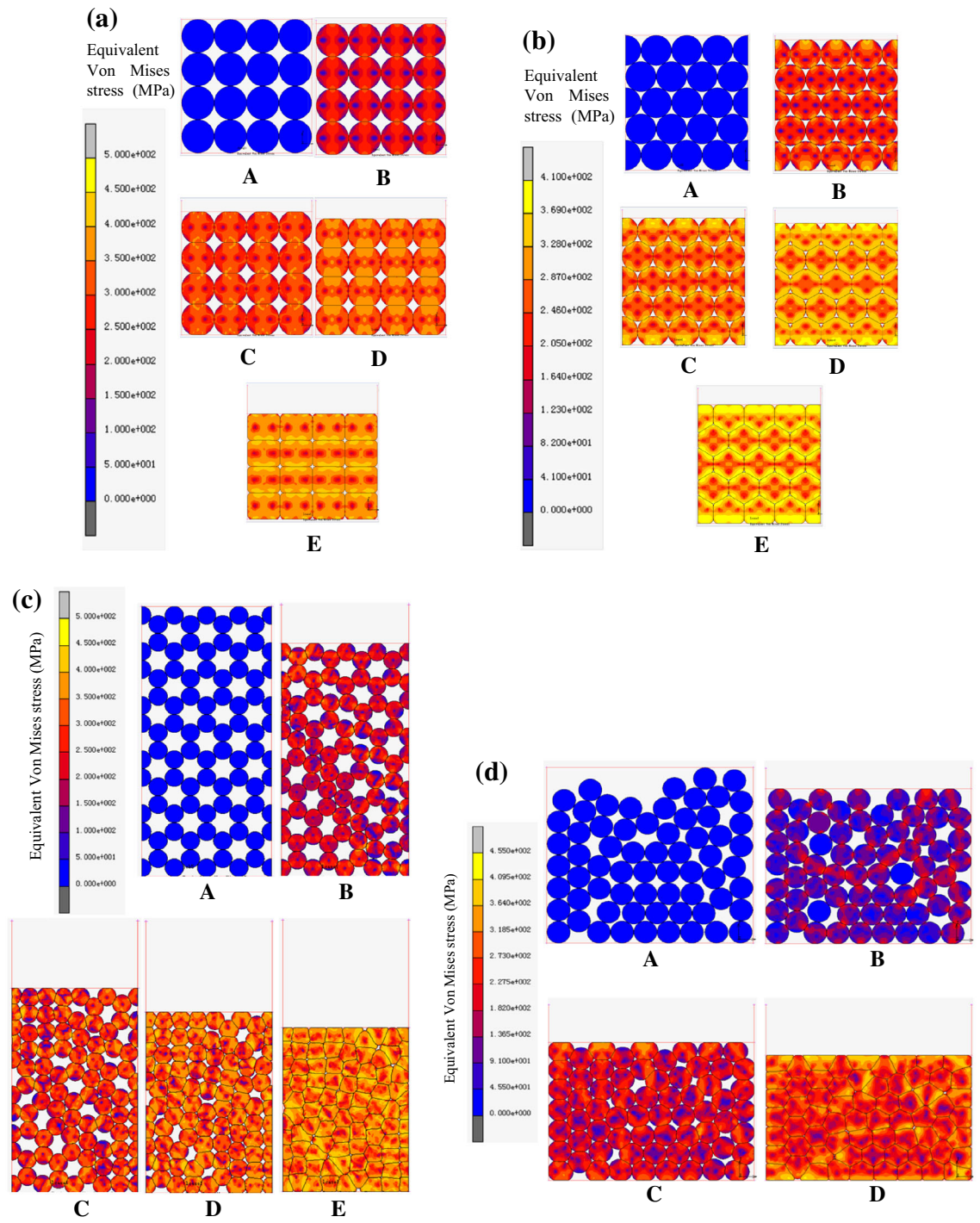

Fig. 4 Evolution of morphology, local packing structure and equivalent Von Mises stress for different initial packing structures during compaction, where: **a** Tetragonal packing: $\rho_A = 0.782$, $\rho_B = 0.801$, $\rho_C = 0.851$, $\rho_D = 0.900$, $\rho_E = 0.986$; **b** HCP: $\rho_A = 0.876$, $\rho_B = 0.899$, $\rho_C = 0.930$, $\rho_D = 0.962$, $\rho_E = 0.989$; **c** Honey comb packing: $\rho_A = 0.602$, $\rho_B = 0.701$, $\rho_C = 0.0.799$, $\rho_D = 0.901$, $\rho_E = 0.990$; **d** Random packing: $\rho_A = 0.714$, $\rho_B = 0.800$, $\rho_C = 0.900$, $\rho_D = 0.990$

modulus, and m—hardening index. Figure 3 shows the fitted results for different initial packing structures. It can be seen that except the honeycomb structure, the fitted results for other three structures indicate high R^2 values, which implies that these numerical results meet the double logarithmic equation. Especially, the compaction on tetragonal and HCP structures indicate very large R^2 value. In comparison, the honeycomb structure with relatively

low R^2 value shows less linearity when the relative density is low. This is determined by its special structure. At the early stage of compaction, the contacts between particles do not evolve continuously, which causes uncertain displacement of some particles. This uncertainty of particle movement cannot be included in the double logarithmic equation. Therefore, the linearity of honeycomb structure shown in Fig. 3 is less than that of other three cases.

3.2 Macrostructure and microstructure characterization during compaction

Figure 4 indicates the evolution of morphology, local packing structure and equivalent Von Mises stress for different initial packing structures during compaction. As shown in Fig. 4a and b, the pressure for tetragonal and HCP initial packings increases rapidly at the early stage of compaction, no obvious relative slip between particles for both cases is observed, and this is determined by the highly geometrical symmetry of the initial packings. Also during compaction, the forces in the two structures are mainly transmitted between neighboring particles located at adjacent layers. At the early stage, the interaction between two particles in contact within the same layer can be very small or negligible, which is in good agreement with our previous results on the force transmission in hard sphere crystal [46]. However, with the further increase in the pressure, large plastic deformation of particles occurred, the in-layer forces between neighboring particles formed and increased. In this duration, the contact between particles changes from point to line, and the large plastic deformation results in the mass transfer of particles to fill adjacent low pressured void area for densification. After compaction, the shapes of particles in the compacts of Fig. 4a and b are rectangles and hexagons, respectively.

Even though honeycomb packing is also the ordered packing structure, however, its densification behavior during compaction is quite different from tetragonal and HCP. As shown in Fig. 4c, at the early stage, with the increase in the pressure, the structure is stable. However, when the pressure is larger than a critical value, relative slip at local area appears which destroyed the ordered structure (see Fig. 4c, B). In this case, the pressure increase is becoming slow compared with tetragonal or HCP compaction, this process continues until the jamming states are formed. Then, the pressure increases rapidly to densify the packing. In the whole process, we can also find some local areas where the stresses on some particles do not increase, which can be regarded as the occurrence of the local slip between particles. After compaction, the shapes of the particles in Fig. 4c are mainly irregular polygons. From force analysis, we find that at early compaction state, the force structure of honeycomb packing is ordered and formed 'Y' type network. Within each particle, the stress distribution is in triangular shape. After the ordered structure is destroyed due to the slip of some particles at higher stress, the contacts and interactions became complicated (see Fig. 4c, B–D). For the compaction of random initial packing in Fig. 4d, the slip begins when the pressure is small. In this stage, particles are rearranged through sliding and rolling to form random dense structure with the relative density of about 0.8, which agrees with others' results in 2D packing [47]. Here, the packing is in jammed state, no obvious deformation of particles is observed. After that, the pressure increases fast and the particles deform plastically with the pressure to form the final dense packing (Fig. 4d, D). Force analysis shows that the forces transmitted from the particle firstly contacted with the punch to its downward neighbors. Then, a clear force chain formed as shown in Fig. 4d, B. During densification, the contacts between particles increase, which leads to the more complex force chain. At the final stage shown in Fig. 4d, D, all the particles are deformed to be different shapes due to the interaction of their neighboring particles.

3.3 Densification mechanism analysis

The densification mechanism during compaction can be ascribed to the filling of interstitial spaces (voids) formed among particles. With the above four initial structures, the compaction mechanism of random initial packing structure is the most complicated due to its anisotropy of void structures (including the shapes and sizes) upon compaction, therefore, we will take this structure as an example to identify its densification dynamics and mechanism. Figure 5 gives the evolution of void structure and corresponding stress distribution for random initial packing upon compaction. It can be seen that at the early compaction stage, particles 'A' and 'B' which formed the 'arching' structure leave a large void underneath. With the influence of stress from neighboring particles, particle 'B' moves to the right side, which provides the condition for the filling of particle 'A'. Then, the particle 'A' is 'pushed' downward by the interaction of its neighboring particles to finish void filling (Fig. 5b, c). Meanwhile, the force chain is changing gradually to form a relatively stable state (Fig. 5d). With the further increase in the pressure, the voids are becoming smaller and smaller due to the large plastic deformation of particles (Fig. 5e), and finally, the dense packing structure is formed as shown in Fig. 5f. Previous theory indicated that the evolution of force chain when the relative density is low can be ascribed to the elasticity and friction among particles [37, 48]; however, Fig. 5 clearly shows that contact yield can occur even at low relative density, which results in the particle sliding during contact deformation.

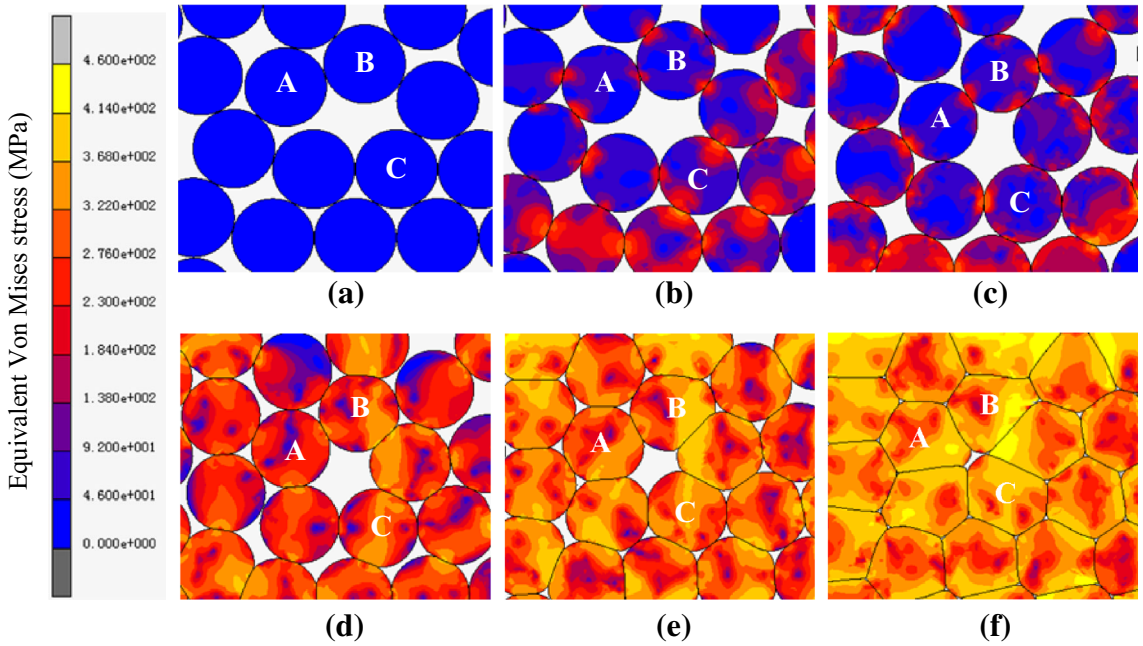

Fig. 5 Evolution of void structure for random packing under compaction and corresponding stress distribution, where: **a** initial packing structure; **b–f** packing structures at 22, 39, 64, 96, and 118 modeling steps, respectively

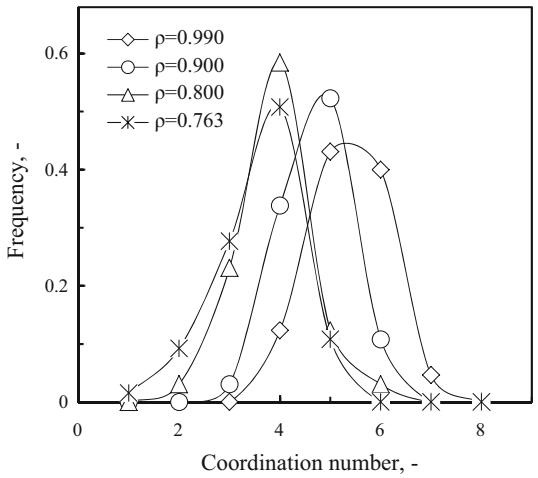

Fig. 6 Coordination number evolution of particles in random initial packing during compaction at different relative densities

Accordingly, we also analyzed the coordination number evolution of particles in the random packing during compaction as shown in Fig. 6. As indicated, with the increase in relative density, the CN distribution shifts to the right, implying more contacts between particles. And at nearly full densification, CN = 5 and CN = 6 are dominant in CN distribution, which means that most of the particles in the final compact are with the shape of pentagon and hexagon. This result is in good agreement with the Voronoi polygon in the packing of spheres [47, 49].

4 Conclusions

Compaction on equal spheres with different initial packing structures such as random packing, tetragonal packing, hexagonal close packed and honeycomb packing in two-dimensional was carried out numerically by MPFEM simulation. The evolution of macro- and micro-properties was characterized and analyzed, and the densification mechanism is identified. Following conclusions are drawn:

(a) For each initial packing structure, the compaction behavior is different. In the compaction of tetragonal and HCP structure, densification is mainly due to the plastic deformation of particles, and no obviously relative sliding between particles is observed. After compaction, the shapes of particles in both compacts are rectangular and hexagonal for tetragonal and HCP structure, respectively. For the compaction of honeycomb and random initial structures, the densification is due to the combination of the deformation under compression and relative sliding and rolling among particles. There is no obvious limit between the deformation and relative sliding. The complicated contacts imply that the final shape of particles in the compact is irregular.

(b) Microscopic analysis on the force behavior indicates that different initial packing structure can lead to different stress distributions in particles and different force chains and transmissions in compacts upon compaction, which will finally determine the final

compact structure and property. Driven by the local stress in the force chain, the particles formed the 'arching' structure were forced to move to fill the large void underneath, then the small voids were filled through mass transfer by plastic deformation of particles around them with the further increase in the pressure.

(c) The discretized mesh division of each particle in FEM model is an effective way to identify the compaction process and densification mechanism from particle scale.

Acknowledgments We are grateful to the financial support of National Natural Science Foundation of China (No. 50974040), China New Century Excellent Talent Funds (NCET-10-0300), and Fundamental research funds for the Central Universities of China (N120202001).

References

1. R.M. German, *Powder Metallurgy Science*, 2nd edn. (Metal Powder Industries Federation, New Jersey, 1994)
2. K. Yamaguchi, N. Takamura, S. Imatani, J. Mater. Process. Technol. **63**, 364 (1997)
3. A.H. Tavakoli, A. Simchi, S.M. Seyed Reihani, Compos. Sci. Technol. **65**, 2094 (2005)
4. K.T. Kim, S.C. Lee, H.S. Ryu, Mater. Sci. Eng. A **340**, 41 (2003)
5. C.A. Leon, G. Rodriguez-Ortiz, E.A. Aguilar-Reyes, Mater. Sci. Eng. A **526**, 106 (2009)
6. M.F. Moreno, C.J.R. González Oliver, Powder Technol. **206**, 297 (2011)
7. D.F. Khan, H.Q. Yin, H. Li, X.H. Qu, M. Khan, S. Ali, M.Z. Iqbal, Mater. Des. **50**, 479 (2013)
8. A.L. Gurson, J. Eng. Mater. Technol. **99**, 2 (1977)
9. E. Arzt, Acta Metall. **30**, 1883 (1982)
10. N.A. Fleck, J. Mech. Phys. Solids **43**, 1409 (1995)
11. P.L. Larsson, S. Biwa, B. Storåkers, Acta Mater. **44**, 3655 (1996)
12. B. Storåkers, N.A. Fleck, R.M. McMeeking, J. Mech. Phys. Solids **47**, 785 (1999)
13. R.J. Henderson, H.W. Chandler, A.R. Akisanya, C.M. Chandler, S.A. Nixon, J. Mech. Phys. Solids **49**, 739 (2001)
14. P. Ponte-Castaňeda, J. Mech. Phys. Solids **50**, 759 (2002)
15. M. Szanto, W. Bier, N. Frage, S. Hartmann, Z. Yosibash, Int. J. Mech. Sci. **50**, 405 (2008)
16. A.T. Procopio, A. Zavaliangos, J. Mech. Phys. Solids **53**, 1523 (2005)
17. D.C. Drucker, W. Prager, Q. Appl. Math. **10**, 157 (1952)
18. D.C. Drucker, R.E. Gibson, D.J. Henkel, Trans. ASCE **122**, 338 (1957)
19. K.H. Roscoe, J.B. Burland, *On the Generalized Stress–Strain Behavior of Wet Clay, ENG PLAST* (Cambridge University Press, Cambridge, 1968)
20. H.A. Kuhn, C.L. Downey, Int. J. Powder Metall. **7**, 15 (1971)
21. S. Shima, M. Oyane, Int. J. Mech. Sci. **18**, 285 (1976)
22. S. Shima, M.A.E. Saleh, Mech. Mater. **16**, 73 (1993)
23. K.T. Kim, S.W. Choi, H. Park, J. Eng. Mater. Technol. **122**, 238 (2000)
24. W. Wu, G. Jiang, R.H. Wagoner, G.S. Daehn, Acta Mater. **48**, 4323 (2000)
25. H. Chtourou, M. Guillot, A. Gakwaya, Int. J. Solids Struct. **39**, 1059–1077 (2002)
26. I.C. Sinka, J.C. Cunningham, A. Zavaliangos, Powder Technol. **133**, 33 (2003)
27. I.C. Sinka, J.C. Cunningham, A. Zavaliangos, J. Pharm. Sci. **98**, 2040 (2004)
28. X.Z. An, R.Y. Yang, K.J. Dong, R.P. Zou, A.B. Yu, Phys. Rev. Lett. **95**, 205502 (2005)
29. A.B. Yu, X.Z. An, R.P. Zou, R.Y. Yang, K. Kendall, Phys. Rev. Lett. **97**, 265501 (2006)
30. X.Z. An, R.Y. Yang, R.P. Zou, A.B. Yu, Powder Technol. **188**, 102 (2008)
31. C.L. Martin, D. Bouvard, S. Shima, J. Mech. Phys. Solids **51**, 667 (2003)
32. O. Skrinjar, P.L. Larsson, *Discrete Element Modeling of Cold Compaction of Composite Powders*. In: Proceeding of the 2002 World Congress on Powder Metallurgy and Particulate Materials (Orlando, FL, USA: MPIF, 2002)
33. C.L. Martin, D. Bouvard, Acta Mater. **51**, 373 (2003)
34. C.L. Martin, D. Bouvard, Int. J. Mech. Sci. **46**, 907 (2004)
35. O. Skrinjar, P.L. Larsson, Comput. Mater. Sci. **31**, 131 (2004)
36. O. Skrinjar, P.L. Larsson, Acta Mater. **52**, 1871 (2004)
37. P. Redanz, N.A. Fleck, Acta Mater. **49**, 4325 (2001)
38. B. Harthong, J.F. Jérier, P. Dorémus, D. Imbault, F.V. Donzé, Int. J. Solids Struct. **46**, 3357 (2009)
39. C. PavanaChand, R. KrishnaKumar, Scr. Mater. **35**, 767 (1996)
40. K.H. Lee, J.M. Lee, B.M. Kim, Trans. Nonferr. Met. Soc. China **19**, s68 (2009)
41. J. Zhang, Compos. Sci. Technol. **69**, 2048 (2009)
42. B. Harthong, J.F. Jérier, V. Richefeu, B. Chareyre, P. Dorémus, D. Imbault, F.V. Donzé, Int. J. Mech. Sci. **61**, 32 (2012)
43. C. Shang, I.C. Sinka, J. Pan, Exp. Mech. **52**, 903 (2012)
44. A.T. Procopio, A. Zavaliangos, J. Mech. Phys. Solids **53**, 1523 (2005)
45. Y.C. Cai, H.H. Zhu, X.Y. Zhuang, Front. Struct. Civ. Eng. **7**, 369 (2013)
46. X.Z. An, F. Huang, AIP Conf. Proc. **1542**, 413 (2013)
47. R.M. German, *Particle Packing Characteristics* (Metal Powder Industries Federation, Princeton, 1989)
48. M. Oda, K. Iwashita, *Mechanics of Granular Materials: An Introduction* (Taylor & Francis Group, 1999)
49. J.L. Finney, Proc. R. Soc. Lond. A Math. Phys. Sci. **319**, 479 (1970)